TEMPERATURE ESTIMATION STUDIES ON INFRARED IMAGES USING RADIOMETRIC APPROACHES

A THESIS SUBMITTED TO
THE GRADUATE SCHOOL OF NATURAL AND APPLIED SCIENCES
OF
MIDDLE EAST TECHNICAL UNIVERSITY

BY

YAĞMUR ATAY

IN PARTIAL FULFILLMENT OF THE REQUIREMENTS
FOR
THE DEGREE OF MASTER OF SCIENCE
IN
DEPARTMENT OF PHYSICS

SEPTEMBER, 2011

Approval of the thesis:

TEMPERATURE ESTIMATION STUDIES ON INFRARED IMAGES USING RADIOMETRIC APPROACHES

submitted by YAĞMUR ATAY in partial fulfilment of the requirements for the degree of **Master of Science in Physics Department, Middle East Technical University** by**,**

Prof. Dr. Canan Özgen _____
Dean, Graduate School **of Natural and Applied Sciences**

Prof. Dr. Sinan Bilikmen _____
Head of Department, **Physics**

Assoc. Prof. Dr. Akif Esendemir _____
Supervisor, **Physics Department, METU**

Examining Committee Members:

Dr. Ali Alaçakır _____
TAEK

Assoc. Prof. Dr. Akif Esendemir _____
Physics Department, METU

Assoc. Prof. Dr. Enver Bulur _____
Physics Department, METU

Assist. Prof. Dr. Sinan Kaan Yerli _____
Physics Department, METU

Prof. Dr. Raşit Turan _____
Physics Department, METU

Date: ___26.08.2011____

I hereby declare that all information in this document has been obtained and presented in accordance with academic rules and ethical conduct. I also declare that, as required by these rules and conduct, I have fully cited and referenced all material and results that are not original to this work.

Name, Surname: Yağmur Atay

Signature:

ABSTRACT

TEMPERATURE ESTIMATION STUDIES ON INFRARED IMAGES USING RADIOMETRIC APPROACHES

Atay, Yağmur

M.Sc., Department of Physics

Supervisor: Assoc. Prof Dr. Akif Esendemir

September 2011, 51 Pages

In this thesis work, temperature estimation algorithms based on physical and radiometric approaches are developed. Developed algorithms, firstly, tested on artificial images for different test cases. Following this, algorithms are tried out on real infrared images in order to verify that they are working properly. Finally, temperature estimations are done by including emissivity. Obtained results are compared to the temperature estimation results of a reference infrared camera. All the results and errors obtained during this study are presented and discussed.

Keywords: Infrared radiation, temperature estimation, radiometric measurements, atmospheric transmission, infrared camera.

ÖZ

KIZILÖTESİ İMAJLAR ÜZERİNDE RADYOMETRİK YAKLAŞIMLAR İLE SICAKLIK KESTİRİMİ

Atay, Yağmur
Yüksek Lisans, Fizik Bölümü
Tez Yöneticisi: Doç. Dr. Akif Esendemir

Eylül 2011, 51 Sayfa

Bu tez çalışmasında, sıcaklık tahmini yapabilmek amacıyla, temeli fiziksel ve radyometrik yaklaşımlara dayanan algoritmalar geliştirilmiştir. Geliştirilen algoritmalar öncelikle yapay bir imaj üzerinde denenmiş, ardından algoritmaların düzgün çalıştığını doğrulamak amacıyla, gerçek kızılötesi resimler üzerinde denenmiştir. Son olarak, sıcaklık tahminleri emisivite değerleri göz önünde bulundurularak yapılmıştır. Elde edilen sonuçlar referans bir kızılötesi kameradan elde edilen sonuçlar ile kıyaslanmıştır. Çalışma boyunca elde edilen tüm sonuçlar, hatalar tartışılmış ve sunulmuştur.

Anahtar Kelimeler: Kızılötesi, sıcaklık kestirimi, radyometrik ölçümler, atmosferik geçirgenlik, kızılötesi kamera.

ACKNOWLEDGEMENTS

I am greatly thankful to my supervisor Assoc. Prof. Dr. Akif Esendemir for his guidance, sharing his experiences and knowledge.

I am very grateful to Assist. Prof. Dr. Sinan Kaan Yerli for his contributions and valuable comments on my study.

I would like to thank my dear colleagues from Roketsan; Koray Ürkmen, Birkan Kurşun and Barış Nurver, for their precious help and for the time we worked together on this study.

I also would like to express gratitude to my parents and my friends for their support, encouragement and understanding. This thesis has never been accomplished without their help and support.

Finally, I would like to thank my dearest fiancé Arda Özertem; for his patience, full support and for the love we share. He always supported and encouraged me, although he is far away from me during this study. Thank you for making me smile and not leaving me alone here. I love you more than anything.

To my parents and my beloved fiancé…

TABLE OF CONTENTS

LIST OF FIGURES

FIGURES

LIST OF TABLES

TABLES

LIST OF ABBREVIATIONS

AT:	Atmospheric Transmission
CFM:	Curve Fit Method
E:	Error
Eqn:	Equation
FIR:	Far Infra Red
GUI:	Graphical User Interface
IR:	Infra Red
LTM:	Look Table Method
LWIR:	Long Wave Infra Red
MODTRAN:	MODerate Resolution Atmospheric TRANsmission
MWIR:	Mid Wave Infrared
NIR:	Near Infra Red
P:	Position
PM:	Planck's Method
ROI:	Region Of Interest
S:	Summer
SWIR:	Short Wave Infra Red
T_{av}:	Average Temperature
VLWIR:	Very Long Wave Infrared
w/:	with
w/o:	without
W:	Winter

CHAPTER 1

INTRODUCTION

1.1 Introduction

Infrared technology was developed firstly for military applications, especially for the need of vision in dark environments. However, infrared technology is now worldwide and IR imagers (or IR cameras) are presented into commercial markets and furthermore, they are used not only for military but also for many different applications (i.e. medical, agricultural, industrial) [1].

Using IR cameras, not only photos or videos of any object can be recorded, but also temperature of the object can be estimated. Estimations can be done by doing some calculations on the image data outputs of IR cameras. To obtain the temperature of an object, a method which is range independent should be developed, since the distance between the object and a camera cannot be measured by using a camera while recording. Temperature measurements can also be done by using IR thermometers (or laser thermometer), however; sometimes false readings can be obtained at ambient temperatures. These errors can occur also due to incorrect emissivity adjustments. Furthermore, these IR thermometers are not suitable for long distant objects and for monitoring large areas.

In this thesis work, a method, which can estimate the temperature of an object by using its IR image, is developed. Generally, IR camera softwares can calculate the temperature of an object whose photo is recorded, however, these temperature results can contain large amount of errors, since camera softwares do not include all

of the parameters, which affect the temperature estimations, during the estimation process.

The method, developed in this thesis work, estimates pixelwise temperature data of a given image by using physical laws for radiometric calculations. It also should be pointed out that developed methods include the parameters (e.g. atmospheric transmission, spectral characteristics of the camera detector and emissivity) which cause attenuation of radiation. IR cameras can supply the raw radiance data of a recorded image. This data can be used for temperature estimations. The estimation methods developed are distance independent (the estimation methods of the commercial IR cameras are also distance independent, i.e. the calculations are done using the radiance values of the image), nevertheless range is taken into account only for atmospheric transmission considerations. The methods add atmospheric transmission and emissivity information to the radiance data, to make more accurate estimations. These methods, which can do more accurate temperature estimations, are considered that they may be used for IR scene modelling or IR signature studies, since they can supply pixel wise temperature data of any source or object.

1.2 Fundamentals of Radiometric Measurements

All materials and bodies emit electromagnetic radiation when its temperature is above absolute zero (0 °K). The radiation represents a conversion of a body's thermal energy into electromagnetic energy, and is therefore called thermal radiation [2]. The working principle of thermal imaging systems depends on detection of the radiant flux distribution of the scene.

In the electromagnetic spectrum, the infrared region lies beyond the visible region up to millimeter (terahertz) waves. Although objects emit radiation across a spectrum of wavelengths, only a particular region of the electromagnetic spectrum is used to gather infrared radiation because of their sensitivity and furthermore photon detectors are able to collect radiation only within a specific waveband because of the atmospheric attenuation [2].

Infrared region is divided into smaller bands and each band has a different name. The boundaries of these bands may change slightly, however a general division is shown below [2];

Near-infrared (NIR): 0.75 – 1.4 μm
Short-wavelength infrared (SWIR): 1.4 – 3 μm
Mid-wavelength infrared (MWIR): 3 – 8 μm
Long-wavelength infrared (LWIR): 8 – 15 μm
Far infrared (FIR) or Very Long Wave Infrared (VLWIR): 15 – 1000 μm

Figure 1 shows the whole electromagnetic spectrum and where the infrared region lies in this spectrum. The studies presented in this thesis work are focused on three main bands, which are SWIR, MWIR and LWIR (SWIR and MWIR bands are used in this study, since the reference IR camera is working in these bands, nevertheless LWIR band is only used for further analysis).

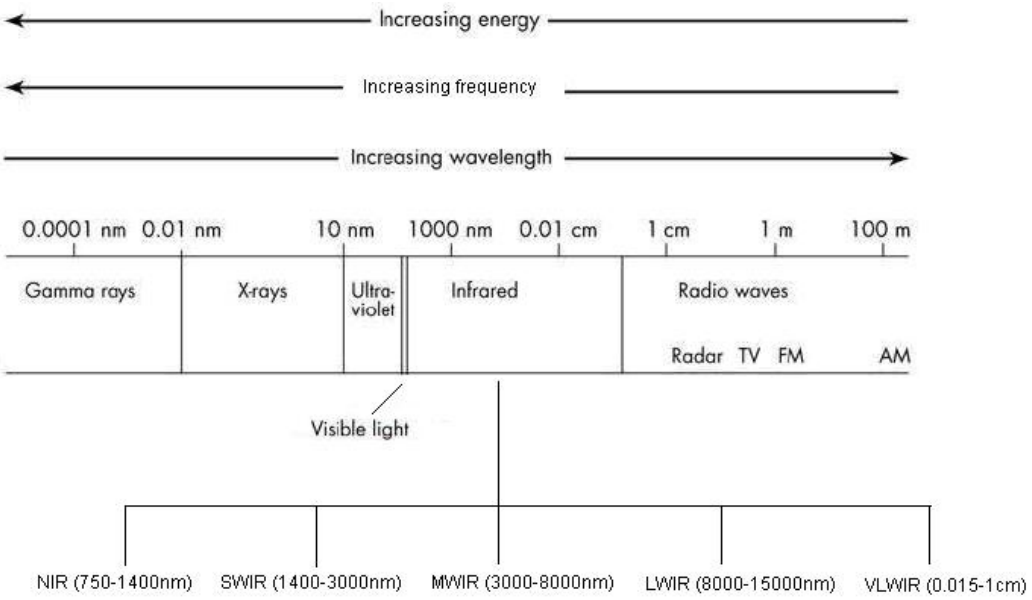

Figure 1 – Electromagnetic spectrum

Infrared radiation emitted by any object can be expressed in several radiometric quantities. The term radiometry deals with measuring electromagnetic radiation in terms of its power, spectral characteristics, temperature, and other parameters

according to source location and detector configuration. In other words, radiometry is used to measure the flux transfer between a source and a sensor. Table 1 shows the radiometric quantities and their units which are used commonly [3].

Table 1 – Radiometric quantities and their units [3]

Radiometric Quantity	Symbol	Unit
Irradiance	E	W/cm^2
Radiance	L	W/cm^2sr
Radiant Intensity	I	W/sr
Spectral Exitance	M_λ	$W/cm^2\mu m$
Total Exitance	M	W/cm^2
Radiance Temperature	T	K
Radiant Flux	Φ	W
Solid Angle	Ω	sr

The quantities, exitance (M), radiant intensity (I) and radiance (L) of an object represent the power emitted at all frequencies from an object surface, whereas irradiance (E) describes the power at all frequencies incident upon a surface. These quantities are illustrated in Figure 2.

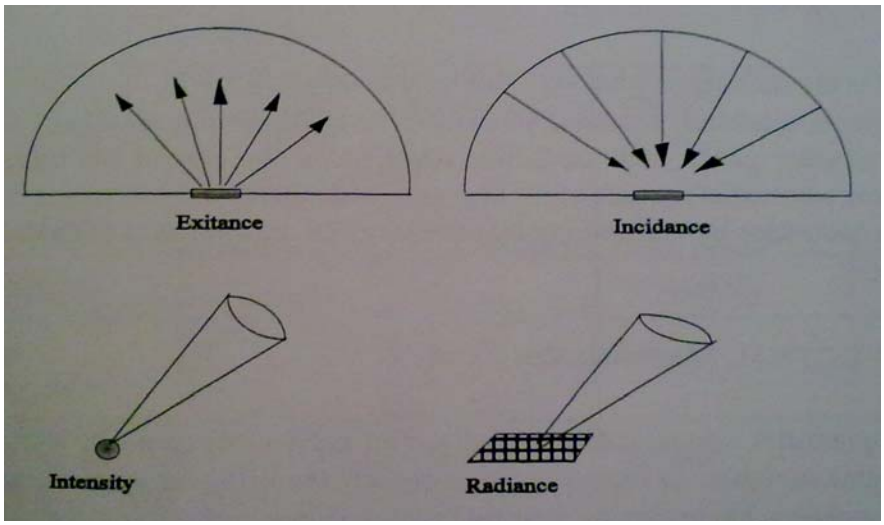

Figure 2 – Illustration of radiometric quantities [4]

Among these radiometric quantities, spectral exitance $M_\lambda(\lambda,T)$ [W/cm^{2}μm], total exitance M [W/cm^2] and radiance L [W/cm^{2}sr] are used in this thesis work, since these parameters are independent of distance (commercial IR cameras also use these parameters for the calculations due to their distance independence).

Planck's radiation law, which is given in Eqn. 1, can be used to calculate the spectral exitance of a source. Here, h denotes the Planck's constant, k denotes the Boltzmann constant and c is the speed of light. This law is also known as the blackbody equation. A blackbody is an object absorbing all the incoming radiation and it is also a perfect radiator according to Kirchhoff's law. It can radiate in a continuous spectrum; however the amount of radiation depends on the body temperature [2].

$$M_\lambda(\lambda,T) = \frac{2\pi hc^2}{\lambda^5}\left[\exp\left(\frac{hc}{\lambda kT}\right)-1\right]^{-1} \text{W}/(cm^2\,\mu m) \qquad \textbf{Eqn. 1}$$

For convenience, Eqn. 1 can be rewritten as [2],

$$M_\lambda(\lambda,T) = \frac{c_1}{\lambda^5}\left[\exp\left(\frac{c_2}{\lambda T}\right)-1\right]^{-1} \left[W/cm^2\,\mu m\right] \qquad \textbf{Eqn. 2}$$

with the following constants,

$c_1 = 3.7410^{-12}$ W cm^2

$c_2 = 14388$ μm K

Integrating Eqn. 2, the total radiant exitance of a blackbody for a given temperature in all wavelengths can be obtained.

$$M = \int_0^\infty M_\lambda(\lambda,T)\,d\lambda = \int_0^\infty \frac{c_1}{\lambda^5}\left[\exp\left(\frac{c_2}{\lambda T}\right)-1\right]^{-1} d\lambda \ \left[W/cm^2\right] \qquad \textbf{Eqn. 3}$$

Figure 3 shows the graph of temperature dependence of the blackbody emission for different temperatures. In Figure 3, Eqn. 2 is plotted for different temperature values from 283.15 °K (10 °C) up to 343.15 °K (70 °C). As seen from the figure that if temperature increases, the spectral exitance also increases and furthermore, the peak emission wavelength is shifted to shorter wavelengths.

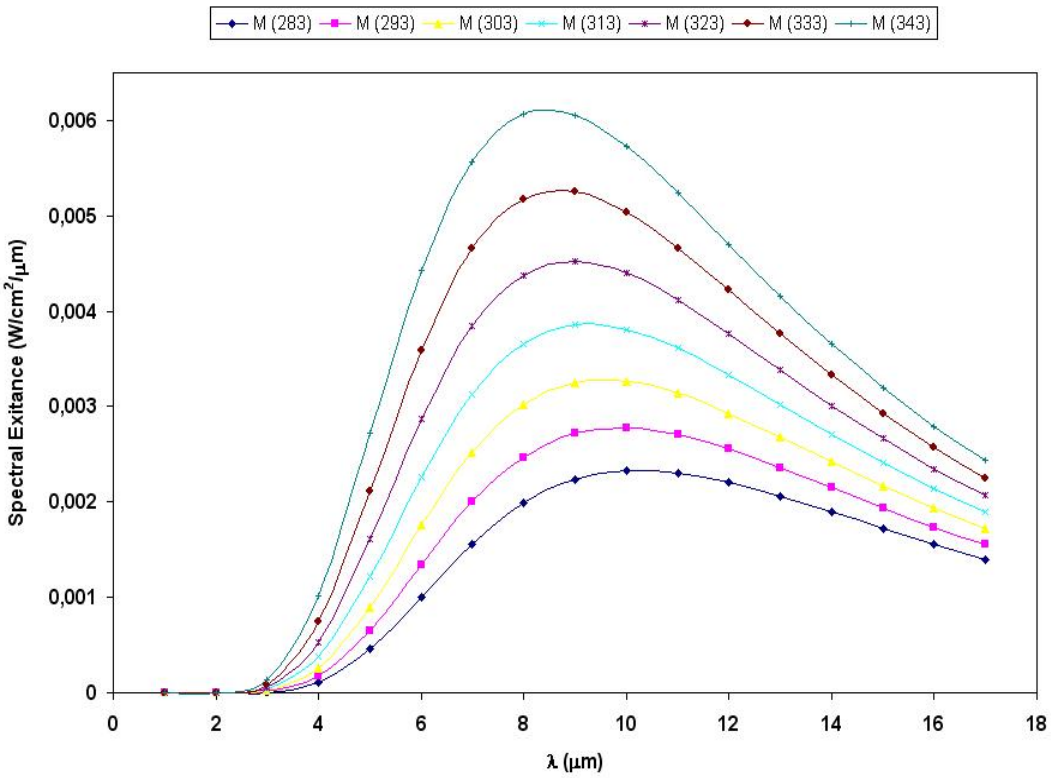

Figure 3 – Blackbody exitance for Planck's law

In this thesis, all the objects and sources are treated as if they are blackbodies.

Since exitance is defined as the radiant flux per unit area, it can also be calculated by using the equation given in Eqn. 4 [4];

$$M = \frac{\Phi}{dA} = \int L(\theta)\, d\Omega_p \quad \left[W / cm^2\right] \qquad \textbf{Eqn. 4}$$

Here, $d\Omega_p$ denotes the projected solid angle. Solid angle which is expressed in Eqn. 5 and shown in Figure 4 is defined as projection of an area onto a sphere divided by square of the radius of the sphere [4].

$$d\Omega_p = \frac{dA\cos(\theta)}{R^2} = \frac{R^2\cos(\theta)\sin(\theta)d\theta d\phi}{R^2} = \cos(\theta)\sin(\theta)d\theta d\phi \quad [sr] \qquad \textbf{Eqn. 5}$$

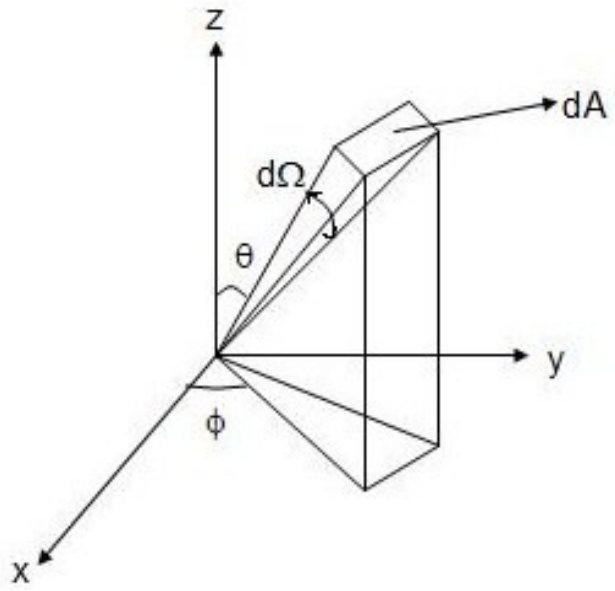

Figure 4 – Representation of solid angle Ω in spherical coordinates

If the source emitting radiation is a Lambertian radiator, meaning that it radiates equal amounts of light in all solid angles, then, the radiance is independent of viewing angle (θ). Using this and inserting Eqn. 5 into Eqn. 4; Eqn. 6 which can be used easy radiance calculations is obtained. Since blackbodies are Lambertian radiators, Eqn. 6 is also valid for them [4].

$$M = \int L d\Omega_p = L\int_0^{\frac{\pi}{2}} \cos(\theta)\sin(\theta)d\theta \int_0^{2\pi} d\phi = L\pi \quad \left[W / cm^2\right] \qquad \textbf{Eqn. 6}$$

It is hard to calculate the total flux coming from any object, since the number of photons per unit area and per unit time, the wavelength of the each emitted photon and the distance between the detector and source should be known for accurate calculations. Because of these reasons, IR cameras also prefer to calculate the radiance of an object, instead of flux. Therfore, calculations done in this thesis work are done by using a similar approach.

All objects are continually emitting radiation at a rate with a wavelength distribution that depends upon the temperature of the object and its spectral emissivity, ε(λ). Emissivity is a measure of a material's ability to radiate absorbed energy. Blackbodies are perfect absorbers and also perfect emitters. A true blackbody would have ε=1, while any real object would have ε<1. The ratio of an object emission to that of a blackbody at the same temperature and in the same spectral interval is defined as the object's emissivity. This definition is given in Eqn. 7 [4].

$$\varepsilon(\lambda) = \frac{M_{object}(\lambda, T)}{M_{blackbody}(\lambda, T)} \qquad \textbf{Eqn. 7}$$

The concept of the blackbody is an idealization, as perfect blackbodies do not exist in nature. However, Graphite (ε=0.98) or human body (ε=0.976) are good examples. Since for all objects except for blackbodies, the emissivity value is less than 1, it decreases the amount of emitted radiation by the object [5]. Therefore, Eqn. 3 becomes;

$$M = \int_0^\infty M_\lambda(\lambda, T)\,\varepsilon(\lambda)\,d\lambda \quad \left[W / cm^2\right] \qquad \textbf{Eqn. 8}$$

An imaging system must view targets through the earth's atmosphere. Before the radiation reaches the sensor, the radiant flux from the target is selectively absorbed by several of the atmospheric gases, and is scattered away from the line of sight by small particles suspended in the atmosphere. The transmittance of a path through

the atmosphere can be expressed as given in Eqn. 9. Here, τ denotes the transmission and σ is the extinction coefficient and x is the path length.

$$T = e^{-\sigma x} \qquad \textbf{Eqn. 9}$$

Under most conditions, absorption and scattering contributes to extinction as;

$$\sigma = \alpha + \gamma \qquad \textbf{Eqn. 10}$$

where α is the absorption coefficient and γ is the scattering coefficient. α and γ are different for each material and they depend generally on wavelength and particle size. Therefore, calculation of transmission is a complicated process.

There are many molecules and particles present in the atmosphere leading to absorption and scattering. These are summarized in Figure 5. To predict the total transmission for a given path length and weather conditions, a software called MODTRAN is used throughout this thesis work.

Contributers to Absorption					
Major	H_2O		CO_2		O_3
Minor	CO	N_2O	O_2	CH_4	N_2
Contributers to Scattering					
Major	CO_2		O_3		N_2
Minor	Fog		Rain		Mist

Figure 5– Atmospheric constituents leading to absorption and scattering [2]

After inclusion the atmospheric transmission to the formula used for exitance, Eqn. 8 becomes,

$$M = \int_0^\infty M_\lambda(\lambda,T)\,\varepsilon(\lambda)T(x,\lambda)d\lambda \quad \left[W/cm^2\right] \qquad \textbf{Eqn. 11}$$

It can be seen from Eqn. 11 that atmospheric transmission depends on both path length and wavelength, however; in Eqn. 9 it depends on the path length and the attenuation coefficient. In fact, the wavelength dependence is embedded in the attenuation coefficient, since the amount of absorption and scattering of the atmospheric constituents changes for each wavelength.

Thermal imagers are used for converting the radiation collected in a specific bandwidth into a single or series of images. Simply, the radiation is emitted by an object with respect to its emissivity, travels through the atmosphere, attenuated by the atmosphere and falls onto a thermal imager's detector. All the phenomena during this travel occur according to physical laws summarized in Chapter 1. In this thesis work, FLIR SC 6000 is used as a reference thermal imager.

Real images have been taken by using FLIR SC 6000 IR camera to compare the results of the artificial image and the real image data. Detailed information of FLIR SC 6000 is given in Appendix.

1.3 Outline

The remaining part of the thesis is organized as follows:

In Chapter 2, how infrared radiation is attenuated and affected by atmospheric transmission will be discussed in detail.

In Chapter 3, generated temperature estimation algorithms, IR camera's estimation algorithms, differences among them and results will be explained.

In Chapter 4, temperature estimation studies including emissivity will be discussed.

Finally, Chapter 5 will be based on the conclusion of this thesis work.

CHAPTER 2

THE EFFECT OF ATMOSPHERIC TRANSMISSION ON INFRARED BANDS

2.1 Atmospheric Transmission Calculations

The effect of atmospheric transmission on infrared radiation is briefly explained in Chapter 1. In this chapter, atmospheric attenuation due to different parameters and the effect of attenuation on infrared radiation will be discussed in detail.

For each specific infrared band used in this thesis work, atmospheric transmission should be calculated and these calculations are done by using MODTRAN. It provides spectral transmittance calculations for arbitrary atmospheric paths from the microwave through the visible bands. A sample graphical user interface of this software is given in Figure 6 [6].

For atmospheric transmission calculations, MODTRAN enables the users to utilize the standard atmospheric and aerosol profiles or users may compose their own profiles by entering the required parameters. These parameters are related to the amount of molecules present in the atmosphere, since the ratio of the atmospheric constituents changes for different regions in the world and for different seasons. Furthermore, aerosol models are used to simulate the effects of dust, clouds, or other particles in the path. Besides, aerosol models can also be composed by the user, like the atmospheric ones [6].

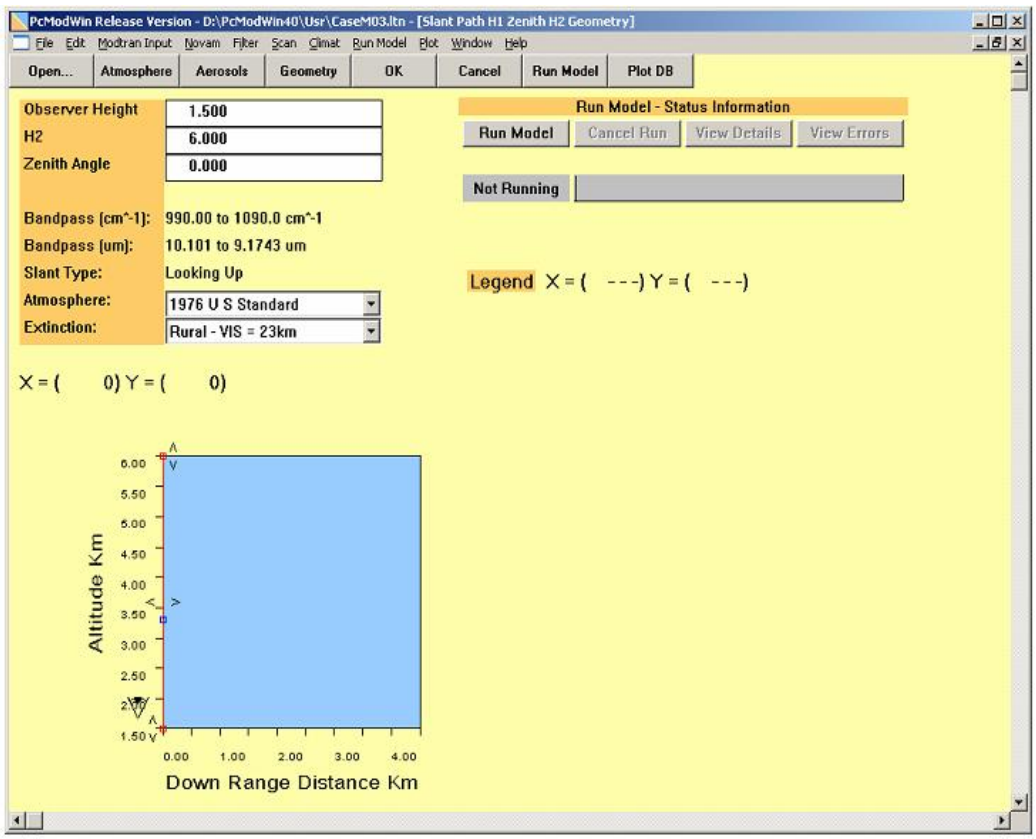

Figure 6 – Sample Modtran GUI [6]

After choosing the appropriate atmospheric profile and the aerosol model, the altitude, path length, path type and required wavelength interval should be entered. Then, the total atmospheric transmission and transmission of the each given molecule is calculated as a percentage by solving many complex differential equations [6]. A typical MODTRAN output file is as shown in Figure 7.

Throughout this thesis work, Midlatitude-Summer and Midlatitude-Winter profiles are used, since they are the most suitable profiles for Turkey in terms of the weather and atmospheric conditions due to its location. No aerosol model is used, since their contributions are assumed to be ignorable (aerosols are the minor contributers to absorption, therefore their contributions are very small). All of the parameters required for transmission calculations are summarized in Table 2.

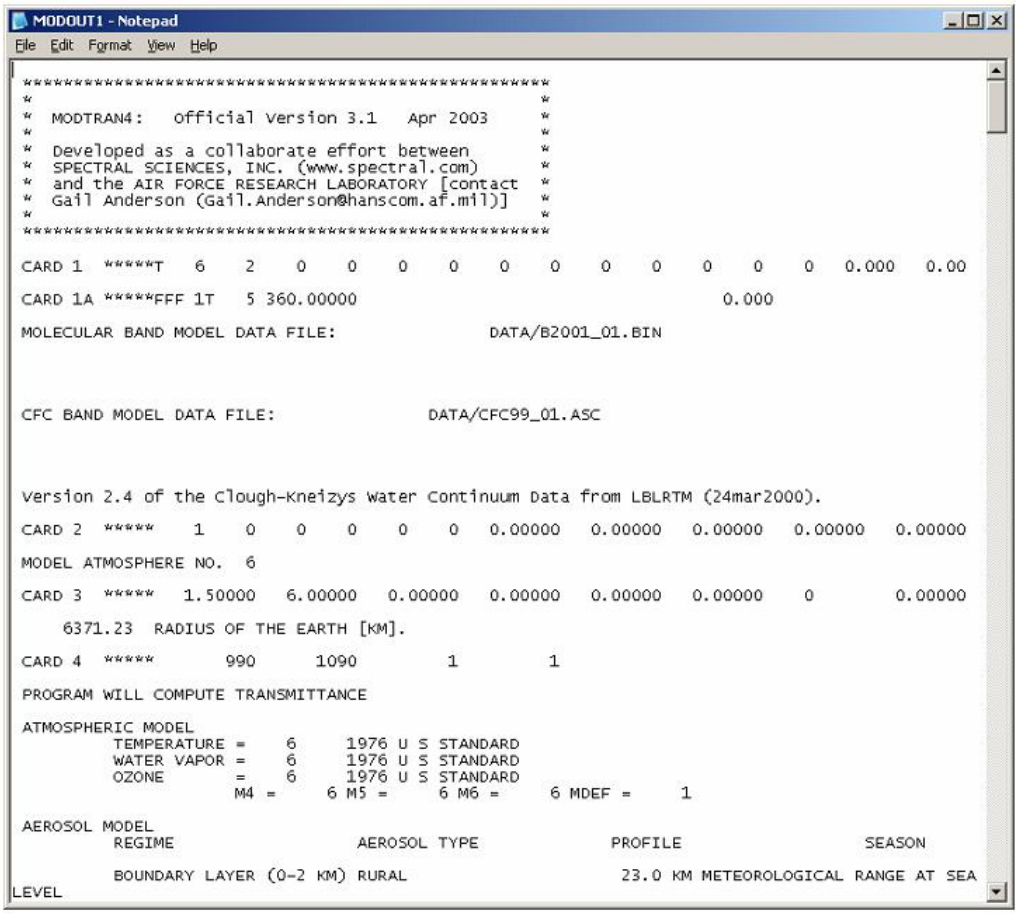

Figure 7 – A typical Modtran output file [6]

Table 2 – Parameters required for transmission calculations

Wavelength intervals:	1.5-5	3-5	8-12
Path lengths:	1km	5km	10km
Altitude:	1m		
Atmospheric profile:	Midlatitude Summer	Midlatitude Winter	
Aerosol model:	No aerosol model		
Path type:	Horizontal		

Three different wavebands, three different path lengths and two different atmospheric profile is used during atmospheric transmission calculations in order to observe and analyze the dependence of atmospheric transmission on different parameters.

2.2 The Effect of Atmospheric Transmission on Infrared Radiation

For each wavelength interval, each different profile and each different path length, atmospheric transmission is calculated by changing the required parameters in MODTRAN. To compare the blackbody emission to the attenuated radiation, graphs were plotted for each different input parameter to observe the amount of attenuation.

For midlatitude atmospheric profiles, for both winter and summer, the transmission values of water (H_2O), carbon dioxide (CO_2) and ozone (O_3) are calculated as default, since they are the major contributing molecules to absorption in IR bands. It can be seen that from Figure 8, that the most and least dominant molecules are water and ozone, respectively. Because of high absorbance of water molecules, in many regions the total transmission is nearly zero. These gaps occurred due to this condition can be seen clearly from the graphs shown in Figure 8. The graphs given in Figure 8 are plotted for a path length of 5 km.

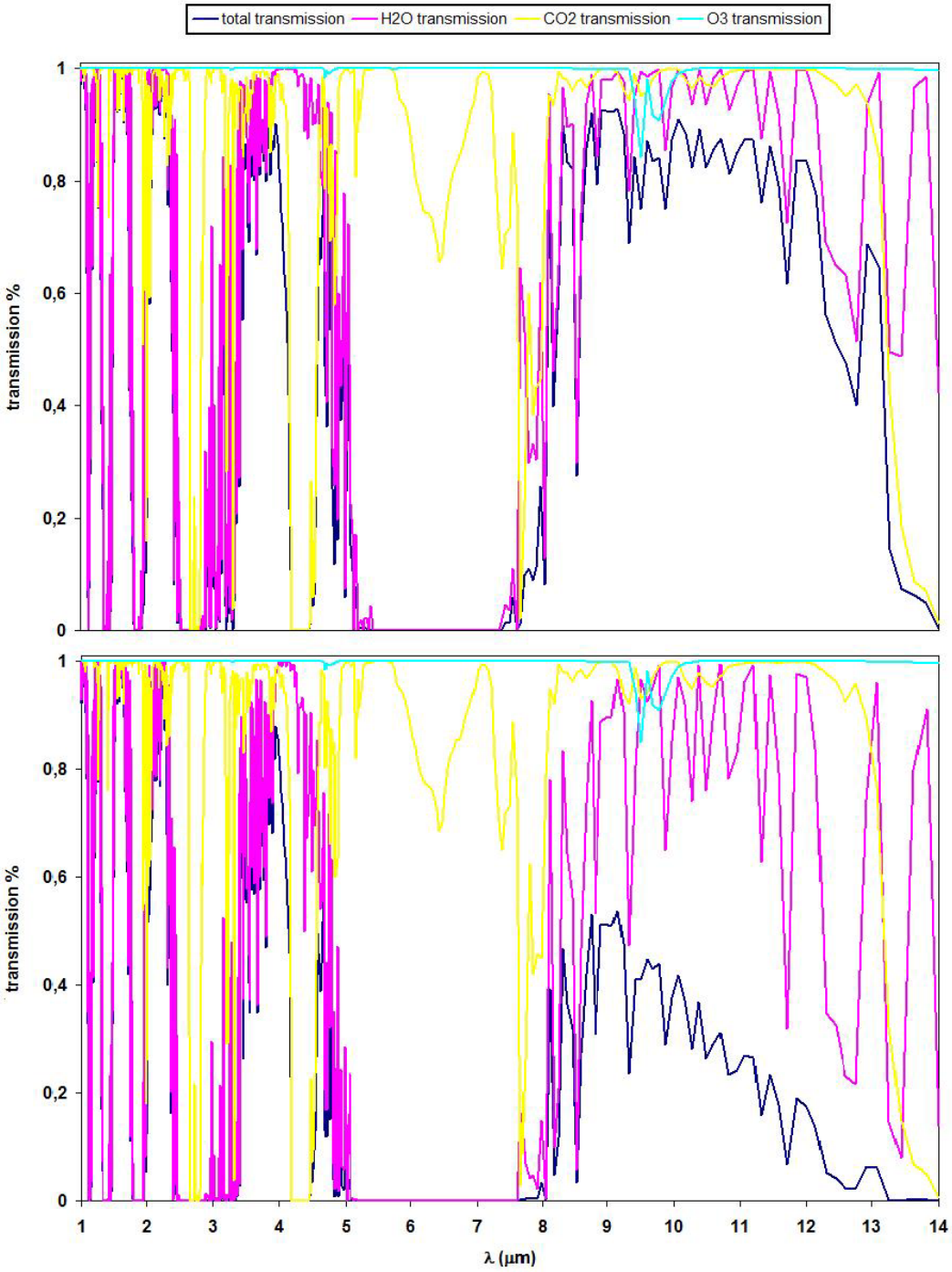

Figure 8 – Atmospheric transmission for midlatitude winter (top panel) and midlatitude summer (bottom panel) profiles at 1 – 14 μm

Transmission also strongly depends on distance. As the distance increases, attenuation occurs more strongly. This dependence can be clearly concluded from Figure 9 and Figure 10. These graphs are formed by multiplying the blackbody's spectral exitance by the obtained total atmospheric transmission values for each three different path lengths. To calculate the blackbody's spectral exitance Planck's Equation given in Eqn. 2 is used. Then, this value is multiplied by the each transmission values of 1 km, 5 km and 10 km, respectively. On the all graphs, the blackbody radiation is attenuated at different amounts with respect to the particular wavelength interval; however, the general behaviour is same. All graphs given in Figure 9 and Figure 10 are plotted for a blackbody at a temperature of 40 °C (313.15 °K).

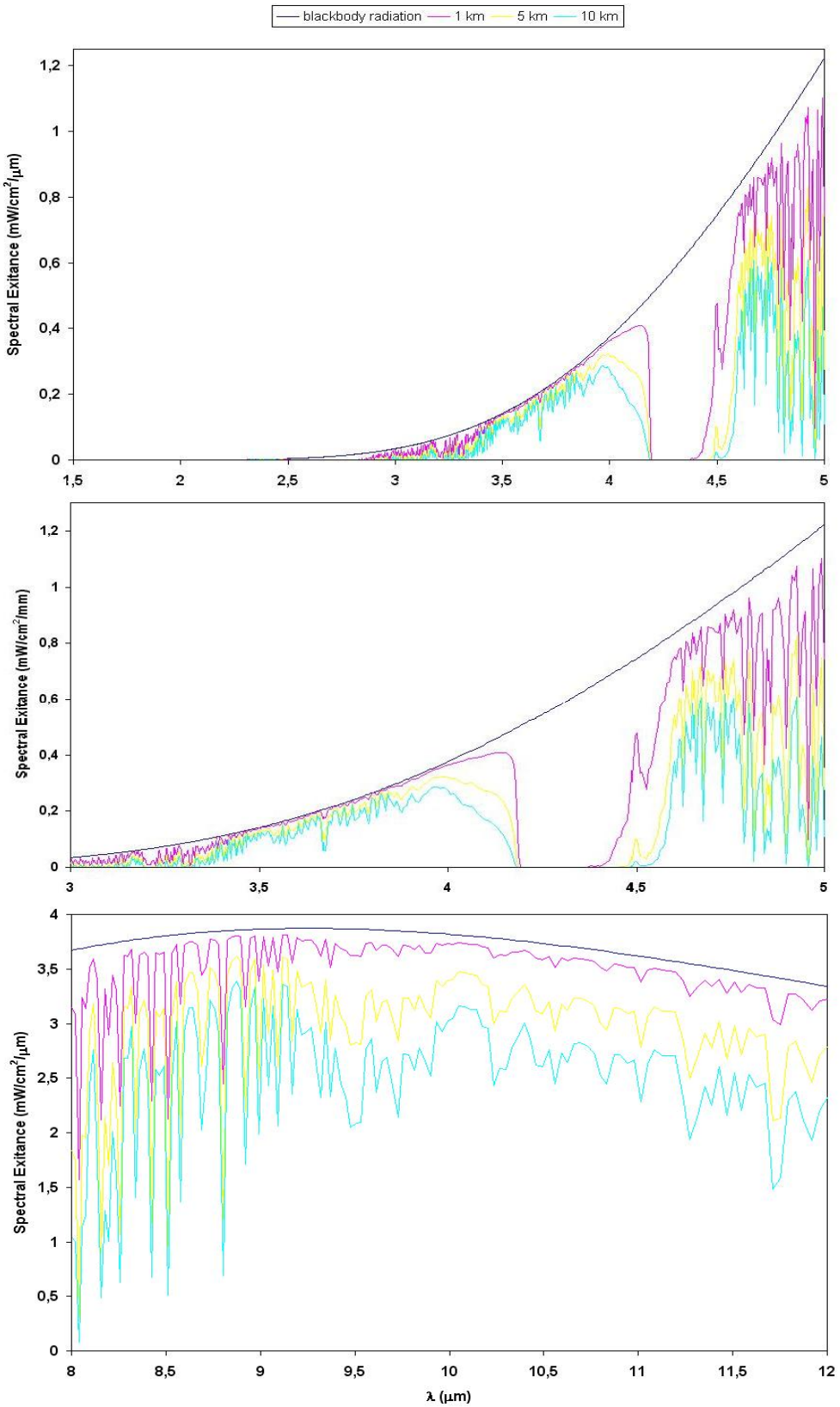

Figure 9 – Attenuation of radiation for Midlatitude-Winter profile at 1,5 – 5 μm (top panel), 3 – 5 μm (middle panel) and 8 – 12 μm (bottom panel) bands for different path lengths

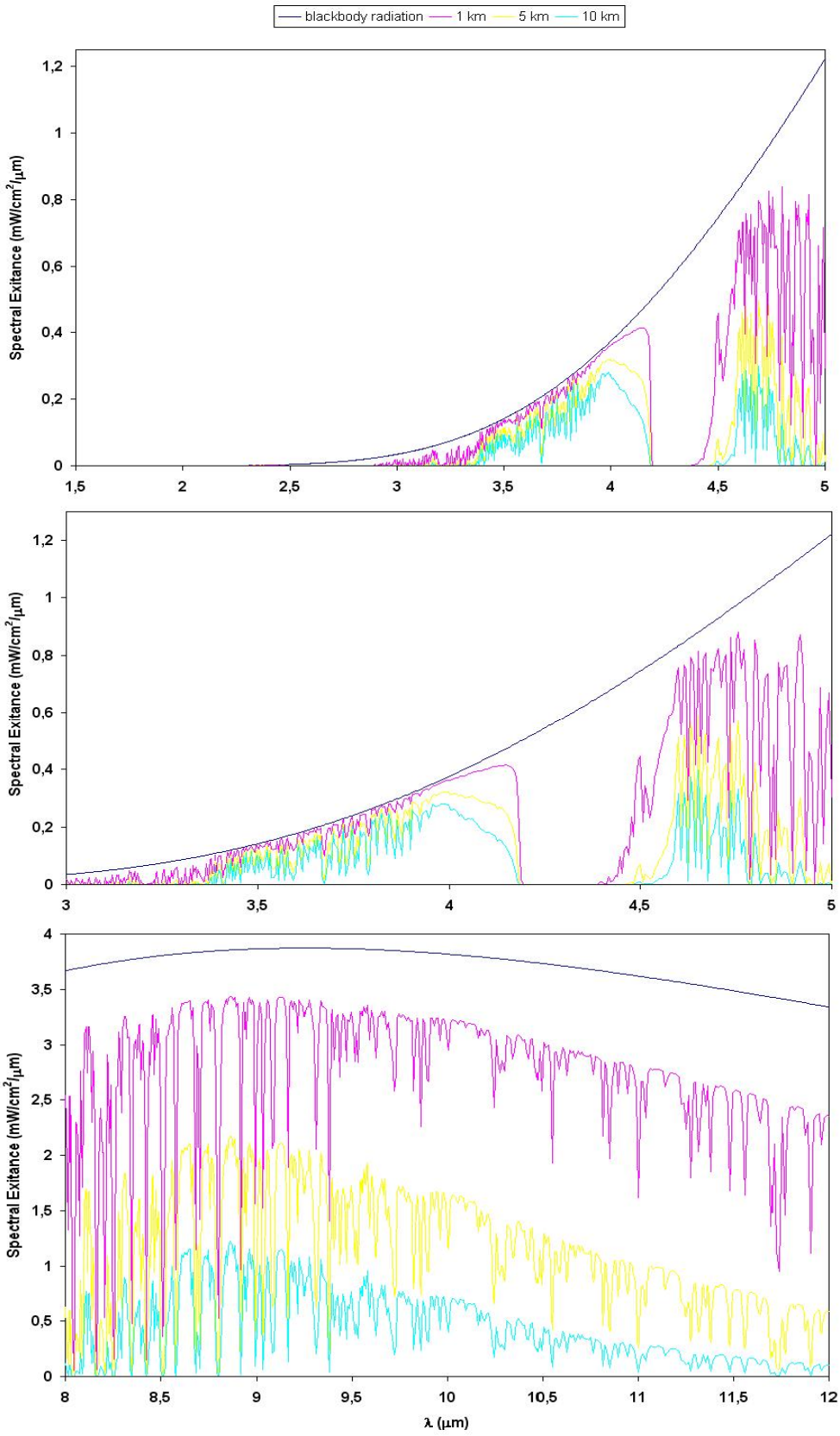

Figure 10 – Attenuation of radiation for Midlatitude-Summer profile at 1,5 – 5 μm (top panel), 3 – 5 μm (middle panel) and 8 – 12 μm (bottom panel) bands for different path lengths

2.3 The Behaviour of Exitance With Respect to Temperature

After examining the relationship between the atmospheric attenuation and range, blackbody radiation vs. temperature relations are studied. According to this study, it has been concluded that, total exitance increases if temperature increases as expected.

Again, for each wavelength interval and for each path length, the blackbody exitance at five different temperatures is calculated. To calculate the spectral exitance, again, Eqn. 2 is used. Then, Eqn. 2 is multiplied by the proper atmospheric transmission and integrated numerically over the each wavelength band at five different temperature values (from 20 °C up to 60 °C) to obtain the total exitance as given in Eqn. 11 ($\varepsilon = 1$).

The relation between temperature and total exitance is shown in the graphs given in Figure 11**,** for 1.5-5 μm, 3-5 μm and 8-12 μm bands, respectively**.**

In each graph given below, the total exitance builds up with the increasing temperature and it decreases with the increasing path length at different amounts. However, it is the same in the all figures that, increment in total exitance according to the increasing temperature is almost linear. No specific analytical dependence is found between these parameters, since the slope of the line differs for each wavelength interval. Using this dependence, temperature estimation algorithms are developed and it is tried to estimate temperature of each pixel of a given infrared image. (this dependence between temperature and total exitance is suitable for using different interpolation methods e.g. linear, cubic and spline, while estimating temperatures).

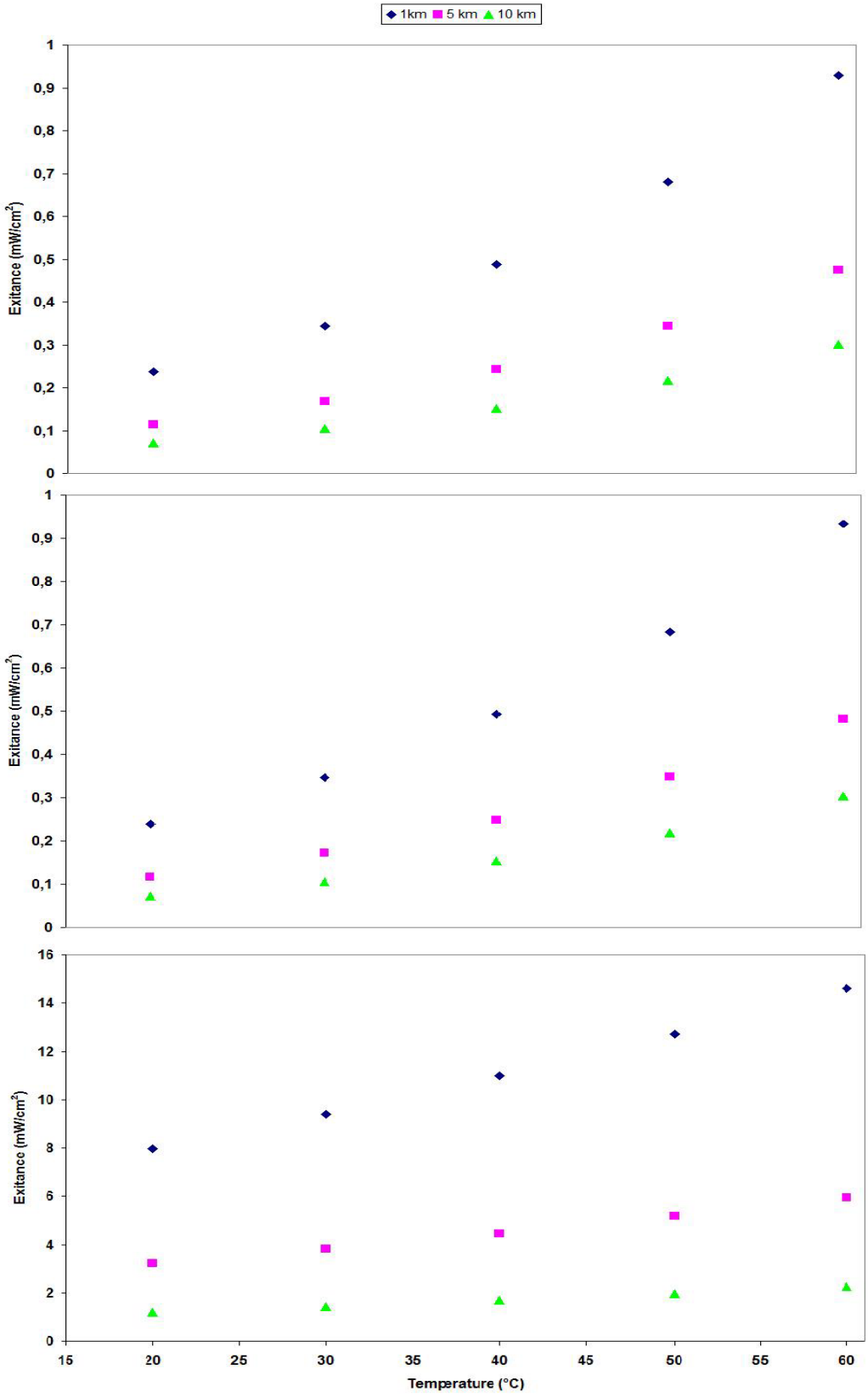

Figure 11 – Temperature dependence of total exitance for 1,5 – 5 μm (top panel), 3 – 5 μm (middle panel) and 8 – 12 μm (bottom panel) bands

CHAPTER 3

TEMPERATURE ESTIMATION ALGORITHMS

3.1 Image Generation

In order to develop temperature estimation algorithms and try them on a given image, an artificial image is formed. For this reason, a simple Gaussian image has been generated using MATLAB. The image has a dimension of 320×240 pixels. The generated image has different temperature values; however, its maximum temperature is 60°C at its center and its minimum temperature value is 8.349 °C. The image and its maximum and minimum temperature values are shown in Figure 12.

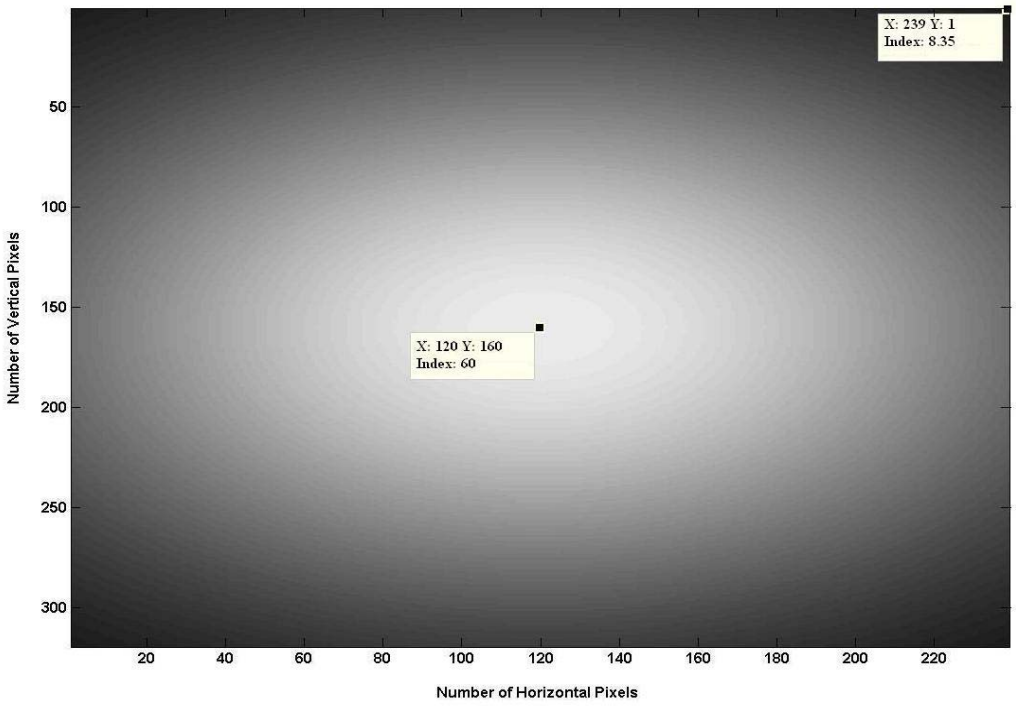

Figure 12 – Generated Gaussian image for temperature estimation algorithms

To create this image the Gaussian distribution function in two dimensions has been used. The function used for the artificial image is given Eqn. 12.

$$f(x) = \exp\left(-\frac{\left(\sqrt{\left((x-\mu)^2 + (y-\mu)^2\right)} \right)^2}{2\sigma^2} \right) \qquad \textbf{Eqn. 12}$$

$\mu = 200$

$\sigma = 100$

where μ is the mean and σ is the standard deviation of the function. According to this function the temperature distribution can be more clearly seen from a 3D plot given in Figure 13.

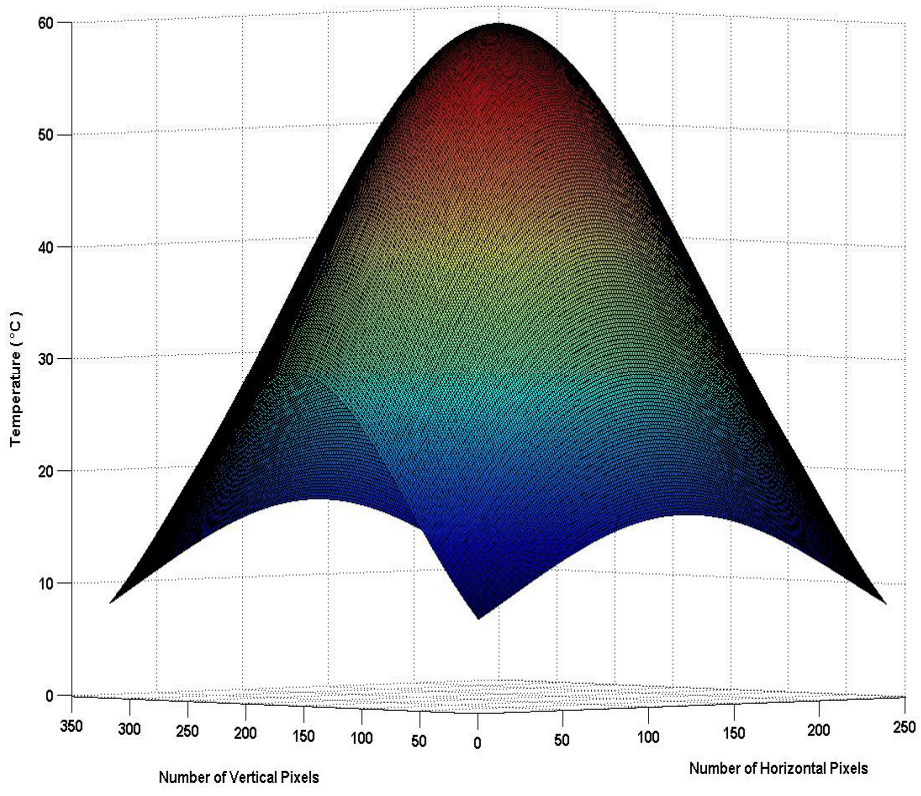

Figure 13 – 3D representation of the temperature distribution of the Gaussian function

This temperature disribution given in Figure 13 is used for the image generation in the desired wavelength intervals.

3.2 Developed Temperature Estimation Algorithms

3.2.1 General Structure of Estimation Methods

In this section, 5 different estimation methods are developed and explained. The general structure of developed estimation algorithms are mainly the same for each method; however they differ in interpolation methods and furthermore they are different in terms of the method of including the atmospheric transmission. The general structure of the algorithms is defined in Table 3.

Table 3 – General structure of the temperature estimation methods

General structure of the algorithms
• Define the wavelength interval • Form a Gaussian image for the desired wavelength interval • Calculate the atmospheric transmission for the defined wavelength interval • Calculate the spectral exitance for each pixel of the generated artificial image • Include atmospheric transmission • Calculate the radiance of each pixel • Estimate the temperature of each pixel (the method of estimation is different for each method)

As defined in the general structure, firstly, the code forms a Gaussian image. After this step, the algorithm calculates the exitance values for each pixel according to the chosen wavelength band. Then, the calculated exitance values are divided by the average atmospheric transmission value using the Modtran output data and finally, these values are converted to radiance. To estimate the temperature of each pixel, a function (referred as *developed function* in Section 3.2.2 and 3.2.3) which also

generates radiance values for temperatures from 0 °C up to 70 °C, is developed. The radiance values calculated in this function do not include atmospheric transmission.

3.2.2 Estimation Methods

1st Method: The general structure of this method is defined in Table 3. After the required calculations and elimination of atmospheric transmission, the radiance values of the each pixel is compared to the radiance values generated by the developed function and the temperature of the closest radiance value is assigned to each pixel.

2nd Method: The general structure of this method is defined in Table 3. After the required calculations and elimination of atmospheric transmission, corresponding temperature values to the radiance values of the artificial image are linearly interpolated from the developed function and these temperature values are assigned to each pixel.

3rd Method: The general structure of this method is defined in Table 3. After the required calculations and elimination of atmospheric transmission, corresponding temperature values to the radiance values of the artificial image are interpolated from the developed function and these temperature values are assigned to each pixel. However, at this time spline interpolation method is used.

4th Method: The general structure of this method is defined in Table 3. After the required calculations and elimination of atmospheric transmission, corresponding temperature values to the radiance values of the artificial image are interpolated from the developed function and these temperature values are assigned to each pixel. However, at this time cubic interpolation method is used.

3.2.3 An Additional Method (5th Method)

5th estimation method is slightly different than other methods in terms of inclusion of atmospheric transmission. However, this method is also generally very similar to other methods in terms of the general structure defined in Table 3. After generating

an artificial image and entering the chosen wavelength interval and Modtran data, the code calculates the exitance values for each pixel. Then, these values are converted to radiance values. Nevertheless, atmospheric transmission is not eliminated during these calculations. Like in the other methods, to estimate the temperature of each pixel, the developed function is used. The main difference appears here, atmospheric transmission is included during the generation of these radiance values in this function and atmospheric transmission is not eliminated in any part of this method. The temperature estimation part is the same as given in the 1st method (temperature comparison is done with the help of the developed function as in the 1st method). Using the radiance values of the each pixel is compared to the radiance values generated by the function and the temperature of the closest radiance value is assigned to each pixel.

The most difficult part of the development of all these algorithms is elimination of atmospheric transmission. As mentioned in Chapter 2, to obtain atmospheric transmission data, Modtran is used. Modtran gives the total spectral atmospheric transmission value and these values are used during the calculation of spectral exitance as given in Eqn. 2. Then, it is numerically integrated for the desired wavelength range as given in Eqn. 13. ε (λ) is ignored for all calculations, assuming that the source behaves like a blackbody (ε = 1).

$$M = \int_{\lambda_1}^{\lambda_2} M_\lambda(\lambda,T)\,\varepsilon(\lambda)T(x,\lambda)\,d\lambda \quad \left[W/cm^2\right] \qquad \textbf{Eqn. 13}$$

The radiance is calculated from the total exitance by using Eqn. 6 in Chapter 1. After converting the exitance values to radiance, it becomes difficult to remove the atmospheric transmission since it depends on many parameters e.g. wavelength, temperature, path length, etc [2]. Even though keeping the parameters constant except for wavelength, does not solve the problem, since estimation process is done on a specific waveband, not on a specific wavelength. The only way to get rid of atmospheric transmission is dividing the radiance value of each pixel to average transmission value. Definitely, this condition causes some amount of errors. To

minimize these errors different interpolation methods are tried for temperature estimation and the results of all these methods are discussed. All of these methods given below are firstly tried on the artificial image and then, they are also tested on real image frames.

3.3 Temperature Estimation Algorithms of the IR Camera

In general, IR cameras cannot directly measure the temperature of an object whose image is being taken. However, the temperature can be calculated approximately using the gathered pixel data of the image. To be able to do this, infrared cameras should be calibrated before use. The user has to enter the temperature and the emissivity of the object during calibration procedure. The detector of the camera can only give a number for each pixel which is proportional to the number of photons falling onto it during the each integration time interval. Since the camera does not know the distance between the object and itself, it can only do radiance calculations, if the user enters the temperature of the object and wavelength interval of the detector through the user interface. This is known as the calibration procedure. The radiance is calculated by using the equations given in Eqn. 6 and Eqn. 13. The other parameters belonging to the camera (e.g. optical transmission of the lenses, spectral response of the detector) which also affect the measurements are also included in calculations; however they are embedded in the camera software.

If the calibration process is done carefully and correctly, the radiance vs. pixel value curve will be quite linear and the temperature estimations will be more accurate.

The IR camera, SC 6000, used for capturing the real images for this thesis work, has three different temperature estimation algorithms [7].

The first estimation is the Planck's method. In this method, using Planck's equations, the temperature is tried to be estimated. The equation used to obtain temperature is derived by using Eqn. 2 and Eqn. 6 and it is given in Eqn. 14. In Eqn. 14, λ_{up} and λ_{down} define the limits of the wavelength band of the IR camera's detector as given in Eqn. 15 [7].

$$Temperature\,(T) = \frac{1.4388 \times 10^4}{\lambda \cdot \ln\left[\left(1.191066 \times 10^4 \cdot \delta \cdot \varepsilon\right)/\left(L(\lambda) \cdot \lambda^5\right) + 1\right]} \qquad \textbf{Eqn. 14}$$

$$\lambda = \frac{\left(\lambda_{up} - \lambda_{low}\right)}{2} + \lambda_{low}$$
$$\delta = \lambda_{up} - \lambda_{low} \qquad \textbf{Eqn. 15}$$

where L(λ) denotes the radiance and ε denotes the emissivity of the object [7].

Second estimation method is the Curve Fit method. During calibration procedure of the IR camera, for every temperature value of a blackbody, radiance is calculated. Accordingly, a temperature vs. radiance curve is generated. Using curve fitting methods on this curve, an equation is tried to be derived to estimate temperature [7].

Third estimation method is the Lookup Table method. Temperature and radiance values recorded during calibration procedure of the IR camera are used in this method. Using these values a lookup table is produced and temperature values are selected and assigned according to this table. If a radiance value of a pixel is between two different radiance values in the lookup table, Eqn. 16 and Eqn. 17 are used to estimate the temperature. [7]

$$percentage = \frac{(RadPixelValue - RadLowerBound)}{\left(RadUpperBound - RadLowerBound\right)} \qquad \textbf{Eqn. 16}$$

$$Temperature = Percentage \cdot \left(TempUpper - TempLower\right) + TempLower \qquad \textbf{Eqn. 17}$$

3.4 Temperature Estimations of the Real Images

All of the five different methods described in Section 3.2 are also used for the temperature estimation of the real images. The difference is that except for the 5th method, atmospheric transmission is not included in the estimation methods. Since the distance between the object and the IR camera was 0.005 km. Average atmospheric transmission is calculated according to Modtran data and it is found as

0.919. Therefore, the atmospheric transmission is assumed to be ignorable and furthermore, during the calibration process of the IR camera, atmospheric transmission is not taken into account, since this process is done in very short distances. Accordingly, it is not taken into account in the 1st, 2nd, 3rd and 4th estimation methods. In Figure 14, the plot of atmospheric transmission data is shown.

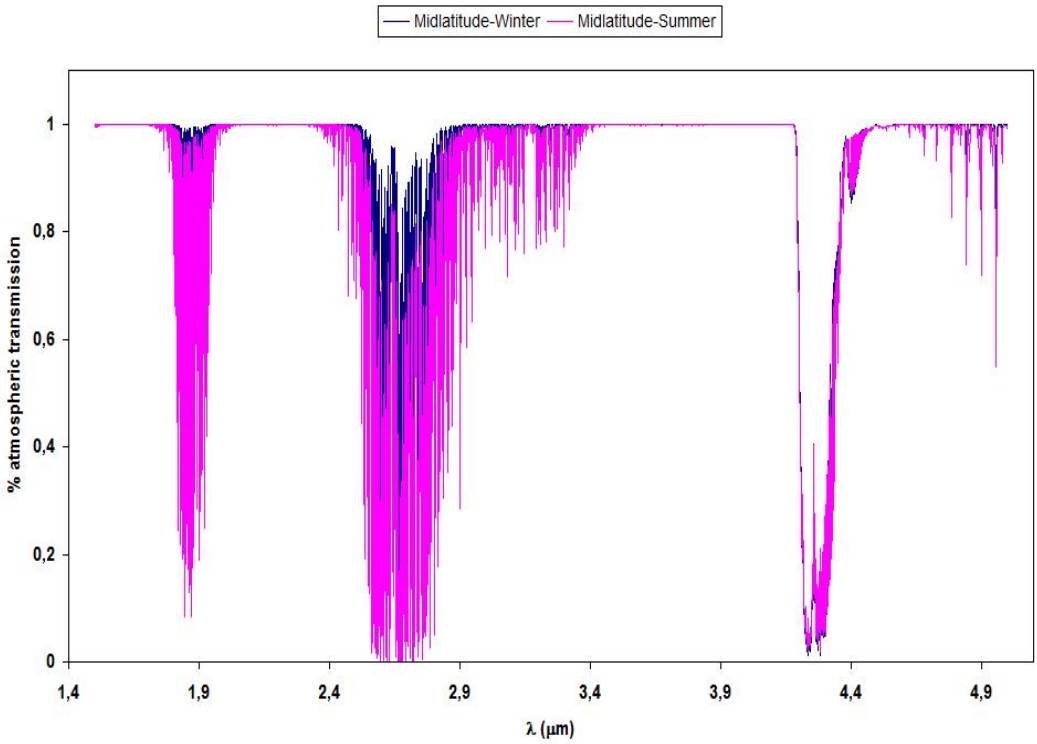

Figure 14 – Atmospheric transmission of 1,5 – 5 μm (path length = 0,005 km)

After recording real images, the IR camera gives 4 different output files for radiance, temperature values of Planck's method, Curve Fit method and Lookup Table method, respectively. Estimated temperatures in this work are compared to all of these 3 estimation results of the IR camera. In all estimation methods, the spectral response of the IR camera which is shown in Figure 15, is also taken into account.

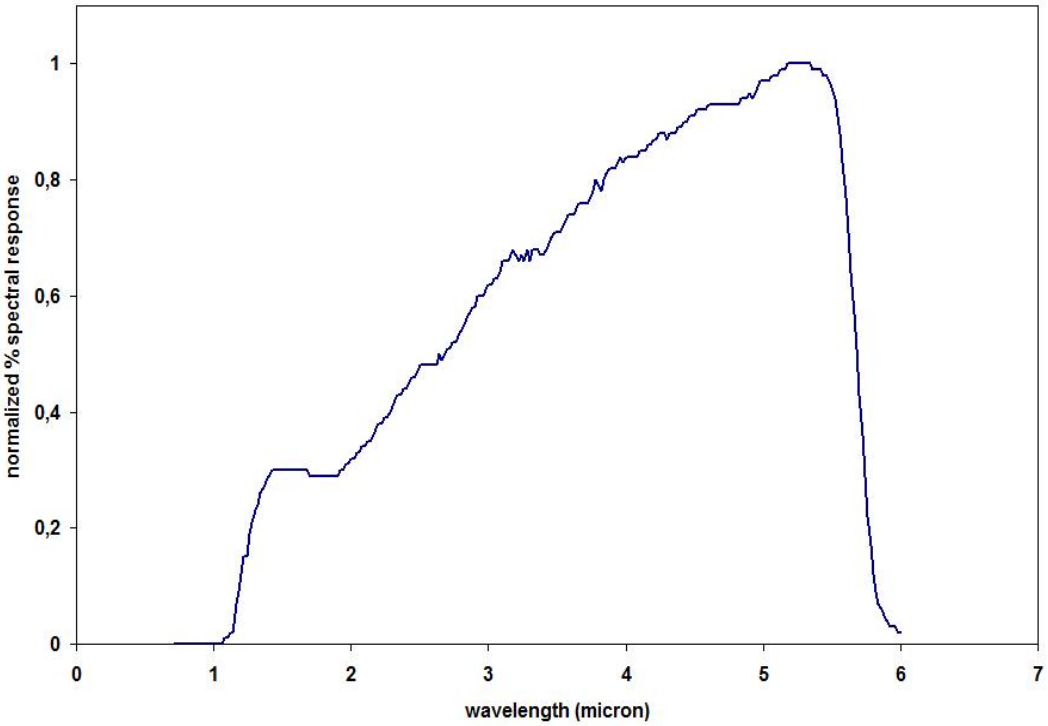

Figure 15 – IR camera's normalized spectral response curve [7]

While recording the images it paid attention to avoid direct sunlight, in order to make more accurate estimations.

3.5 Error Results of the Estimation Methods

The results of the temperature estimation algorithms of the all methods discussed in Section 3.2 are shown in Table 4 for 1.5-5 μm, 3-5 μm and 8-12 μm, respectively. Minimum and maximum temperature errors are given in all tables for both Midlatitude-Summer and Midlatitude-Winter atmospheric profiles. For all of the test cases the path length is taken as 5 km for atmospheric transmission calculations. In Table 4; the amount of errors, obtained while estimating the temperature, is shown for both cases, without including atmospheric transmission and including atmospheric transmission, respectively (first two rows given for each profile show the amount of error obtained without including the atmospheric transmission). Without adding atmospheric transmission to the calculations, it can be observed

from Table 4, that the maximum error equals to 1 °C for 1st, 2nd, 3rd and 4th method (in the 5th method, radiance without atmospheric transmission is not calculated). However, the amount of error increases if atmospheric transmission is added to the calculations and the amount of error is not common for each method, since the effect of atmospheric transmission cannot be removed completely due to its wavelength dependence. Nevertheless, although different amount of errors are obtained in each method for different bands and profiles, the amount of error obtained in the 5th method is around 1 °C for each case.

Temperature estimation results of the real images are given in Table 5. In this table, temperature errors obtained in each developed method with respect to each estimation method of the IR camera are revealed. Furthermore, the results of more than one frame are given in Table 5 in order to justify that the estimation algorithm to work properly for each frame.

If the results of the real image estimations are evaluated with respect to camera's estimation methods, the amount of error obtained in Curve Fit Method and Lookup Table Method (the errors obtained for Curve Fit Method and Lookup Table Method are very close to each other) is lower than that of in Planck's Method. This shows that the results obtained for each method of the IR camera do not measure the same temperature for the same point and furthermore, the measured temperatures for each method are not consistent with each other. Accordingly, this result can cause problems, since at this point, the user of the camera has to decide about which result is more accurate.

Best results obtained for temperature values are highlighted in lightgray and darkgray for the results without including atmospheric transmission and including atmospheric transmission, respectively in Table 4. In Table 5 best results obtained for real image estimations are also highlighted in lightgray.

Table 4 – Error results (+/-) of five different temperature estimation algorithms in 1.5-5 μm (top panel), 3-5 μm (middle panel), 8-12 μm (bottom panel) bands in both Summer and Winter at mid-lattitudes. All values are in ^{o}C. Abbreviations: E: Error, S: Summer, W: Winter, AT: Atmospheric Transmission.

		1st	2nd	3rd	4th	5th
S (w/o AT)	**E_{max}**	1.000	0.004	0.000	0.000	
S (w/o AT)	**E_{min}**	0.996	0.000	0.000	0.000	
S (w/ AT)	**E_{max}**	14.369	15.369	15.366	15.366	1.000
S (w/ AT)	**E_{min}**	8.349	13.631	13.411	13.276	0.995
W (w/o AT)	**E_{max}**	1.000	0.004	0.000	0.000	
W (w/o AT)	**E_{min}**	0.995	0.000	0.000	0.000	
W (w/ AT)	**E_{max}**	6.580	7.580	7.577	7.577	1.000
W (w/ AT)	**E_{min}**	5.206	6.206	6.204	6.204	0.996
S (w/o AT)	**E_{max}**	1.000	0.004	0.000	0.000	
S (w/o AT)	**E_{min}**	0.996	0.000	0.000	0.000	
S (w/AT)	**E_{max}**	5.114	6.114	6.111	6.111	1.000
S (w/ AT)	**E_{min}**	4.359	5.359	5.356	5.356	0.995
W (w/o AT)	**E_{max}**	1.000	0.004	0.000	0.000	
W (w/o AT)	**E_{min}**	0.996	0.000	0.000	0.000	
W (w/ AT)	**E_{max}**	2.332	3.332	3.328	3.328	1.000
W (w/ AT)	**E_{min}**	2.218	3.218	3.216	3.216	0.996
S (w/o AT)	**E_{max}**	1.000	0.001	0.000	0.000	
S (w/o AT)	**E_{min}**	0.998	0.000	0.000	0.000	
S (w/ AT)	**E_{max}**	0.242	1.177	1.176	1.176	1.000
S (w/ AT)	**E_{min}**	0.000	0.758	0.757	0.757	0.998
W (w/o AT)	**E_{max}**	1.000	0.001	0.000	0.000	
W (w/o AT)	**E_{min}**	0.998	0.000	0.000	0.000	
W (w/ AT)	**E_{max}**	2.121	1.121	1.121	1.121	1.000
W (w/ AT)	**E_{min}**	2.079	1.079	1.081	1.081	0.998

Table 5 – Error results (+/-) of the real image estimations in 1.5-5 μm band for frame 1 (top panel), frame 2 (middle panel) and frame 3 (bottom panel) with respect to the reference IR camera's estimation algorithms for five different temperature estimation methods. All values are in ^{o}C. Abbreviations: E: Error, PM: Planck's Method, CFM: Curve Fitting Method, LTM: Lookup Table Method.

		1st	2nd	3rd	4th	5th
PM	E_{max}	9.357	10.357	10.354	10.354	2.862
	E_{min}	6.216	7.216	7.214	7.214	0.000
CFM	E_{max}	1.406	0.406	0.406	0.406	8.599
	E_{min}	1.241	0.241	0.244	0.244	7.812
LTM	E_{max}	1.323	0.323	0.323	0.323	8.634
	E_{min}	1.301	0.301	0.304	0.304	7.799
PM	E_{max}	9.355	10.356	10.352	10.352	2.861
	E_{min}	6.176	7.176	7.173	7.173	0.000
CFM	E_{max}	1.406	0.406	0.406	0.406	8.616
	E_{min}	1.241	0.241	0.244	0.244	7.814
LTM	E_{max}	1.323	0.323	0.323	0.323	8.648
	E_{min}	1.302	0.302	0.305	0.305	7.801
PM	E_{max}	9.515	10.515	10.514	10.514	3.071
	E_{min}	6.153	7.153	7.151	7.151	0.000
CFM	E_{max}	1.406	0.406	0.406	0.406	8.624
	E_{min}	1.241	0.241	0.244	0.244	7.711
LTM	E_{max}	1.323	0.323	0.323	0.323	8.654
	E_{min}	1.301	0.301	0.304	0.304	7.760

3.6 Error Analysis

According to the results given in Section 3.5, pixelwise error analysis is done and the amount of maximum and minimum errors is tried to be identified. In this section, error analysis is done and maximum and minimum errors are tried to be

located. The error positions are given in Table 6 (position of errors in terms of temperature) and Table 8 (position of errors in terms of pixel locations), for the artificial image (1.5 μm, 3-5 μm, 8-12 μm bands) and real images, respectively.

For the estimations done on the artificial image; generally, maximum errors observed at the maximum temperature value and similarly, minimum errors observed at the minimum temperature of the artificial image. The maximum and minimum temperature limits of the artificial image are given already in Section 3.1. Nevertheless, in some test cases, the opposite condition is observed exceptionally. However, it can be inferred from the results given in Table 6 that the maximum and minimum amount of errors are generally observed at the extremum temperature values. Here, the main problem is that Table 4 and Table 6 do not give any information about the error distribution between the minimum and maximum temperature limits. Accordingly error analysis is required and for this purpose test cases are selected randomly. The error distribution for randomly chosen wavebands and atmospheric profiles is given in Figure 16 and Figure 17. According to the results, the error distribution differs for each waveband and also for each atmospheric profile. From the 3-5μm/Midlatitude-Winter, 1.5-5 μm/Midlatitude-Winter and 1.5-5 μm/Midlatitude-Summer graphs, it can be said that the amount of error increases with the increasing temperature. However, if the 8-12 μm/Midlatitude-Summer case is examined, it can be concluded that there is not any general tendency for the error amount occurred during estimations. If 1.5-5μm/Midlatitude-Winter and 1.5-5μm/Midlatitude-Summer graphs are compared, it can be seen that error distribution also differs for different atmospheric profiles at the same waveband.

Maximum amount of error is observed at 1.5-5 μm waveband. The reason behind this condition is considered that elimination of atmospheric transmission becomes harder for 1.5-5 μm, since this band is broadest band among 1.5-5 μm, 3-5μm and 8-12μm, therefore the fluctuation of atmospheric transmission is seen for this band more frequently and it causes larger amount of errors during averaging process of atmospheric transmission as given before in Figure 9 and Figure 14.

Nevertheless, a general result can be concluded from the below graphs. The behaviour of error distribution belonging to the 5th method is very similar and consistent for different wavebands (the amount of error is around 1 °C for all test cases) and different atmospheric profiles. From Figure 16 and Figure 17, it can be also observed clearly, the error distribution of 5th method is almost constant (the slope of the line is very small) for different temperature values. Furthermore, from Table 6, Figure 16 and Figure 17**,** it can be observed that the maximum and minimum amount of errors are occurred at the same temperature values for each waveband and atmospheric profile, meaning that the results of the 5th method is very consistent for each test case.

Table 6 – Position (in terms of temperature) of maximum and minimum errors obtained in the artificial image estimations for 1.5 – 5 μm (top panel), 3-5. μm (middle panel) and 8-12μm (bottom panel) bands. All values are in ^{o}C. Abbreviations: E:Error, P: Position, S: Summer, W: Winter

	1st	**2nd**	**3rd**	**4th**	**5th**
S/P of E_{max}	60.000	60.000	60.000	60.000	60.000
S/P of E_{min}	8.349	13.633	8.349	8.349	8.483
W/P of E_{max}	60.000	60.000	60.000	60.000	60.000
W/P of E_{min}	8.349	8.349	8.349	8.349	8.483
S/P of E_{max}	8.349	8.349	8.349	8.349	60.000
S/P of E_{min}	60.000	60.000	60.000	60.000	8.483
W/P of E_{max}	46.829	46.8289	47.264	47.394	60.000
W/P of E_{min}	8.349	8.349	8.349	8.349	8.483
S/P of E_{max}	60.000	8.349	8.349	8.349	60.000
S/P of E_{min}	30.931	60.000	60.000	60.000	8.483
W/P of E_{max}	59.880	59.881	60.000	60.000	60.000
W/P of E_{min}	8.349	8.349	8.349	8.349	8.483

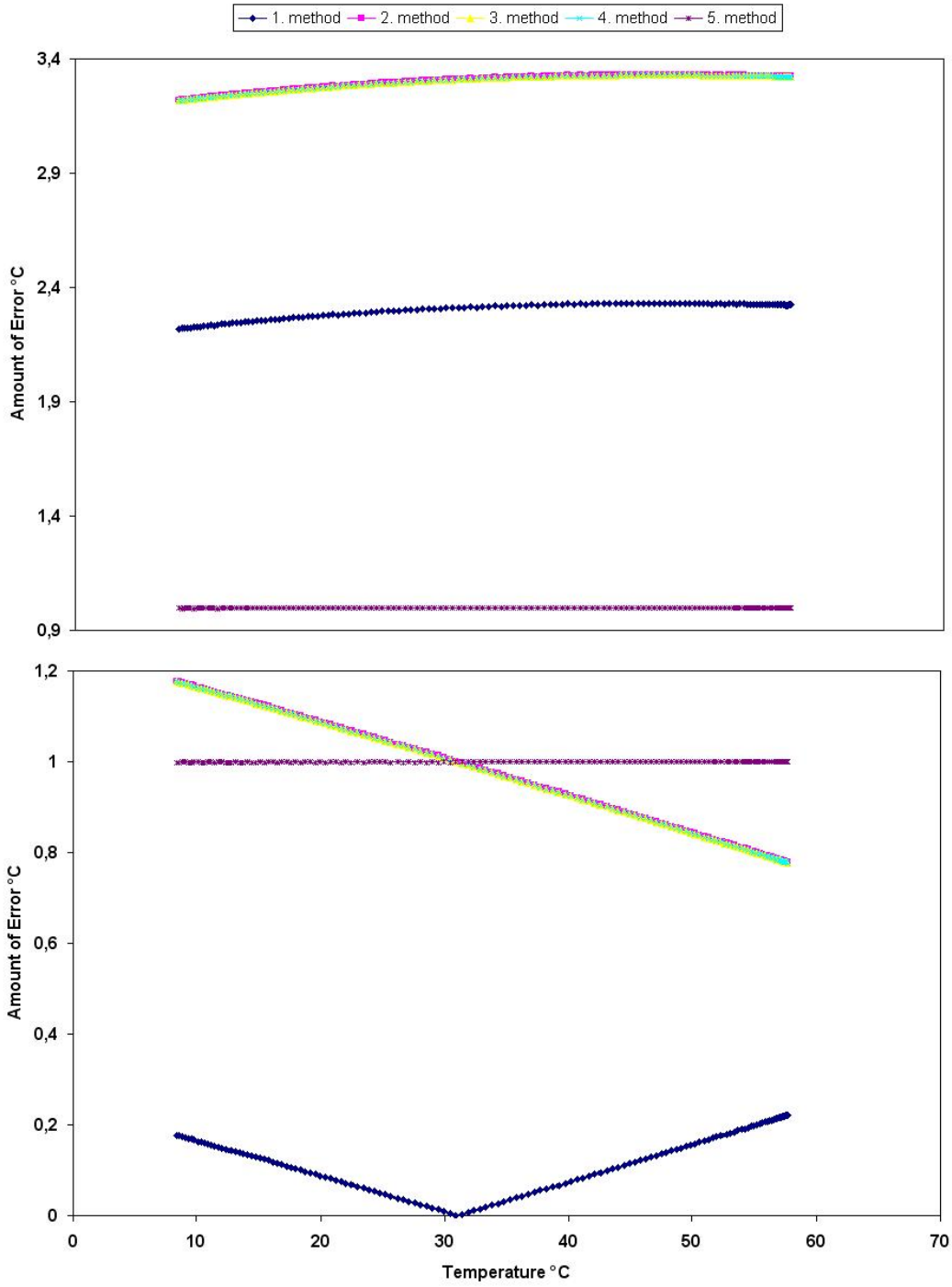

Figure 16 – Error distribution for 3 – 5 μm/ Midlatitude-Winter (top panel) and 8 – 12 μm/ Midlatitude-Summer (bottom panel)

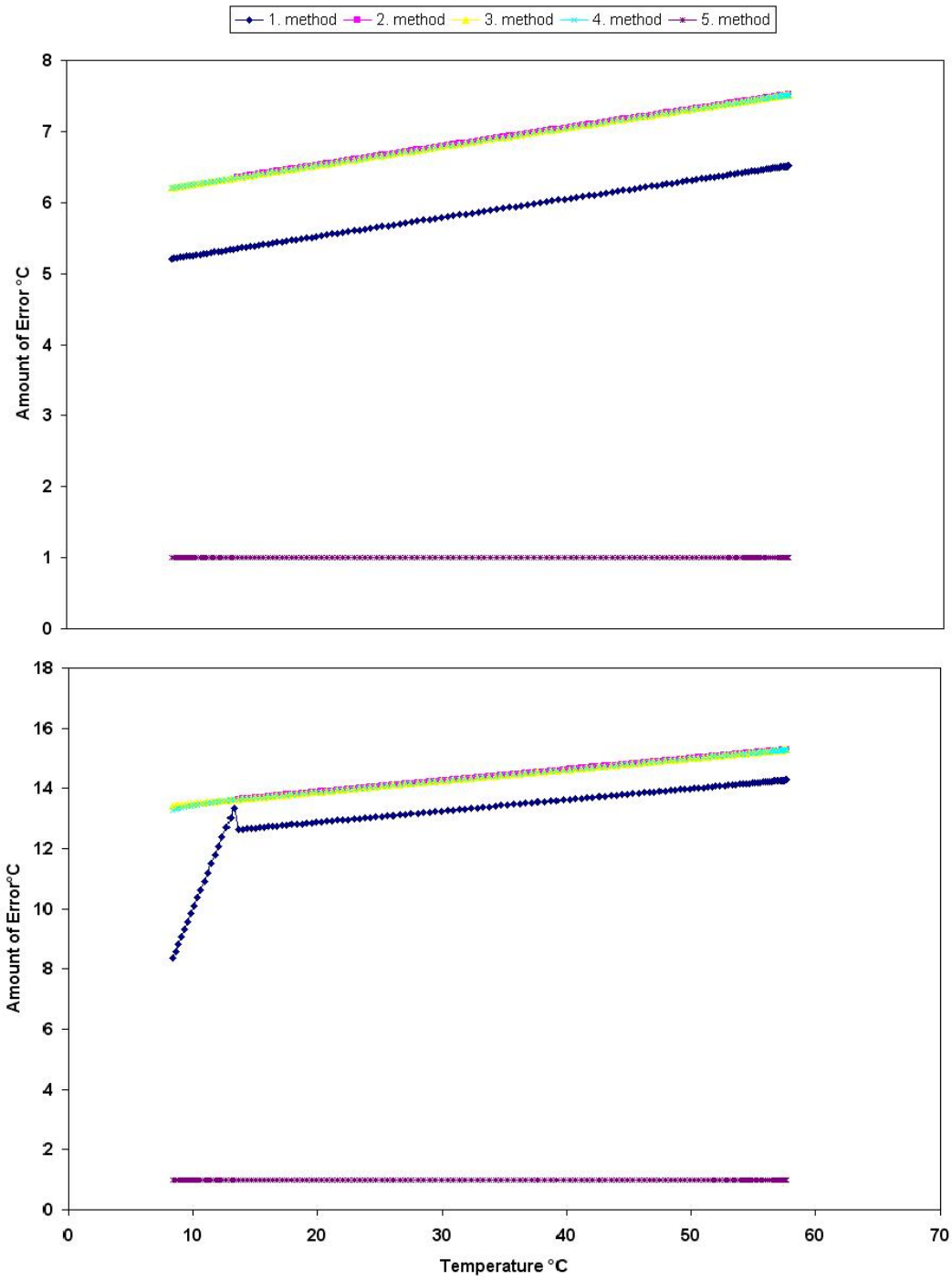

Figure 17 – Error distribution for 1,5 – 5 μm band midlatitude-winter (top panel) and 1,5 – 5 μm band midlatitude-summer (bottom panel)

Position of maximum and minimum errors occurred in the real image estimations are given in Table 8. Since real image estimations are done on three different frames and each frame has different temperature limits and different temperature distributions, pixel numbers are used to locate the maximum and minimum errors

instead of temperature values (for the artificial image estimations temperature values are used to locate the minimum and maximum errors). The maximum and minimum temperature limits of the real image frames for each estimation method of the IR camera are shown in Table 7.

If results given in Table 8 are evaluated together with the reference temperature data given in Table 7, a similar error distribution is also observed for the real image estimations. In general, maximum and minimum amount of errors are observed again around the extremum temperature values of each frame; however, exceptions can be also observed again for some cases. Furthermore, no common tendency can be defined for error occurrence between the temperature limits.

The maximum and minimum errors occurred during real image estimations are shown in Figure 18, Figure 19, Figure 20, for each frame and each method (the pixel numbers given in Table 8 are circled in the figures to locate the errors on the real image frames).

Table 7 – Maximum and minimum temperature limits measured by IR camera's estimation algorithms. All values are in ^{0}C. Abbreviations: PM: Planck's Method, CFM: Curve Fitting Method, LTM: Lookup Table Method.

		Frame 1	Frame 2	Frame 3
PM	**Max.**	50.408	50.741	50.926
	Min.	23.960	23.959	22.448
CFM	**Max.**	42.907	43.277	43.484
	Min.	13.286	13.284	11.666
LTM	**Max.**	42.873	43.245	43.453
	Min.	13.299	13.297	11.617

Table 8 – Position of maximum and minimum errors obtained for frame 1 (top panel), frame 2 (middle panel) and frame 3 (bottom panel). Abbreviations: PM: Planck's Method, CFM: Curve Fitting Method, LTM: Lookup Table Method, E: Error, P: Position.

		1st	2nd	3rd	4th	5th
PM	**P of E_{max}**	231x426	231x426	231x426	231x426	231x426
	P of E_{min}	208x52	208x52	208x52	208x52	215x294
CFM	**P of E_{max}**	455x363	455x363	485x371	485x371	208x52
	P of E_{min}	236x149	236x149	194x240	194x240	231x426
LTM	**P of E_{max}**	207x47	207x47	207x42	207x42	208x52
	P of E_{min}	233x423	233x423	233x429	233x429	231x426
PM	**P of E_{max}**	225x423	225x423	225x423	225x423	225x423
	P of E_{min}	207x51	207x51	207x51	207x51	229x42
CFM	**P of E_{max}**	181x357	181x357	434x635	434x635	207x51
	P of E_{min}	208x338	208x338	110x79	110x79	225x423
LTM	**P of E_{max}**	214x115	214x115	206x49	206x49	207x51
	P of E_{min}	227x426	227x426	227x426	227x426	225x423
PM	**P of E_{max}**	459x492	459x492	459x492	459x492	459x492
	P of E_{min}	208x51	208x51	208x51	208x51	113x206
CFM	**P of E_{max}**	451x358	451x358	469x399	469x399	207x46
	P of E_{min}	117x55	117x55	190x605	190x605	459x492
LTM	**P of E_{max}**	110x12	110x12	209x48	209x48	207x46
	P of E_{min}	458x492	458x492	458x492	458x492	459x492

Figure 18 – Position of minimum and maximum errors in Frame 1 for Planck's Method (top panel), Curve Fit Method (middle panel), Lookup Table Method (bottom panel) All values are in ^{o}C.

Figure 19 – Position of minimum and maximum errors in Frame 2 for Planck's Method (top panel), Curve Fit Method (middle panel), Lookup Table Method (bottom panel) All values are in ^{o}C.

Figure 20 – Position of minimum and maximum errors in Frame 3 for Planck's Method (top panel), Curve Fit Method (middle panel), Lookup Table Method (bottom panel) All values are in ^{o}C.

CHAPTER 4

TEMPERATURE ESTIMATION STUDIES INCLUDING EMISSIVITY

4.1 The Method of Including Emissivity in Estimation Algorithms

The main concept of emissivity is given before in Section 1.2. Estimation studies with emissivity are done only on the real images, since an object or material, whose emissivity value (it is taken $\varepsilon(\lambda) = 0.976$ by average as given also in Section 1.2) is a known parameter, is necessary [8]. For this reason, human skin is chosen. The emission profile of human skin is similar to a blackbody, in other words it is almost wavelength independent [8]. The temperature of human skin is also a known parameter, which provides commenting on the amount of error done by the estimation algorithms.

To include emissivity in the algorithms, a ROI (Region of Interest) is selected for each image frame. In these ROIs, it is tried to be covered only the human face. Each ROI is chosen specifically for each frame. After choosing the ROI, emissivity should be included inside these ROIs. Consequently, Eqn. 8 given in Section 1.2 can be used. Since the emissivity of human skin is almost wavelength independent (similar to blackbodies), Eqn. 8 can be rewritten as;

$$M = \int_{\lambda_1}^{\lambda_2} M_\lambda(\lambda,T)\,\varepsilon(\lambda)\,d\lambda = \varepsilon \int_{\lambda_1}^{\lambda_2} M_\lambda(\lambda,T)\,d\lambda \quad \left[W/cm^2\right] \qquad \textbf{Eqn. 18}$$

After obtaining total exitance to calculate the radiance similar to other estimation methods, Eqn. 6 can be used with the inclusion of emissivity. Therefore, Eqn. 6 becomes,

$$L = \frac{M\varepsilon}{\pi} \quad \left[W / cm^2 / sr\right] \qquad \textbf{Eqn. 19}$$

4.2 Estimation Results

The estimation results including emissivity are given in Table 9, for each method and for three different frames. To form this table, firstly the average temperature within a ROI without including emissivity is calculated. Secondly, emissivity is included in the estimation algorithms and again, average temperature is calculated. Both results are shown in Table 9. In Figure 21, the boundaries of ROIs chosen for each individual frame are shown. In the developed algorithms, for every frame the pixel locations of the selected ROI should be entered in order to estimate the average temperature including emissivity. To illustrate, for Frame 1 the selected ROI constitutes of horizontal and vertical pixels, from 173 to 230 and from 375 to 417, respectively and these values are entered for calculations.

As seen from the results, in each method, the temperature values are increased by 1 °C to 2 °C with the inclusion of emissivity compared to the estimations without emissivity as expected. If the results of the each method are examined, it can be seen from Table 9 that the results of the 5th method are very close to average human skin temperatures which are known around 34 °C (34 °C is the temperature value measured at the forehand) [9]. According to the results, the amount of error obtained in the 5th method is around 3 °C with respect to the reference temperature (human skin temperature). It can be also inferred that the estimated temperatures in each frame are very close to each other.

Best results are highlighted in Table 9 for each frame in lightgray.

Furthermore, IR camera's estimations including emissivity are also examined in order to compare them to the results of the developed methods (same ROIs are used for each frame in order to make a more accurate comparison). According to the IR camera results given in Table 10, it can be observed, again, that the results obtained in each method are inconsistent with each other (the results obtained for Curve Fit and Lookup Table Methods are very close to each other). In addition, the amount of error range changes between ± 3.5 °C – 5.5 °C, which is larger than the error value obtained in the 5th method.

Table 9 – Temperature estimation results on real images without/with emissivity for frame 1 (top panel), frame 2 (middle panel) and frame 3 (bottom panel). All values are in ^{o}C. Abbreviations: T_{Av}: Average Temperature

	1st	**2nd**	**3rd**	**4th**	**5th**
T_{Av} (w/o ε)	28.928	27.928	27.929	27.929	35.816
T_{Av} (w/ ε)	30.201	29.201	29.201	29.201	37.125
T_{Av} (w/o ε)	29.135	28.135	28.137	28.137	36.029
T_{Av} (w/ ε)	30.409	29.409	29.409	29.409	37.339
T_{Av} (w/o ε)	29.181	28.181	28.184	28.184	36.077
T_{Av} (w/ ε)	30.457	29.457	29.457	29.457	37.388

Figure 21 – Selected ROIs of frames 1-3 (left to right)

Table 10 – Average temperature results of IR camera's estimation methods within the ROIs including emissivity for frame 1 (top panel), frame 2 (middle panel) and frame 3 (bottom panel). All values are in ^{o}C. Abbreviations: PM: Planck's Method, CFM: Curve Fit Method, LTM: Lookup Table Method, T_{Av}: Average Temperature

Frame 1	**T_{Av} in PM:**	37.677
	T_{Av} in CFM:	28.612
	T_{Av} in LTM:	28.597
Frame 2	**T_{Av} in PM:**	38.138
	T_{Av} in CFM:	29.134
	T_{Av} in LTM:	29.115
Frame 3	**T_{Av} in PM:**	38.181
	T_{Av} in CFM:	29.183
	T_{Av} in LTM:	29.163

CHAPTER 5

CONCLUSION

In this thesis work, pixelwise temperature estimation methods on an IR image are studied. All of the developed methods are based on physical laws and approaches. The purpose of developing these methods is estimating the temperature of any object present in an IR image including the spectral characteristics of the detector, atmospheric transmission and emissivity. Since commercial IR cameras can do estimations without including these parameters and accordingly estimated temperatures contain large amount of errors.

In this study, five different estimation methods are developed and presented. The main idea and the general structure of the algorithm behind these methods are similar; however, they differ from each other in terms of interpolation methods and the method of including atmospheric transmission.

As explained detailed before, removal of atmospheric transmission from exitance is very hard, since it is a function of wavelength. Therefore, in order to get rid of the effect of atmospheric transmission, calculated exitance values are divided by the average transmission values (except for 5^{th} method). Because of this condition, a certain amount of error is added to radiance values. To minimize these errors, different interpolation methods are used in each estimation method. Developed estimation methods are firstly tested on an artificial image. After that, these developed algorithms are tested on different real IR images. These real images recorded by using the FLIR SC 6000. The software of this IR camera can also estimate the temperature of the images by using several methods. The results of developed temperature algorithms are compared to the results of these methods.

All of the five methods are tested on 6 different test cases (1.5-5 μm/Midlatitude-Summer, 1.5-5 μm/Midlatitude-Winter, 3-5 μm/Midlatitude-Summer, 3-5μm /Midlatitude-Winter, 8-12 μm/Midlatitude-Summer, and 8-12 μm/Midlatitude-Winter are the test cases). According to the results of error analysis, in the 1st, 2nd, 3rd and 4th method, the maximum error equals to ±1°C for the radiance calculation without including the atmospheric transmission (radiance without atmospheric transmission is not calculated in 5th method) for each waveband. However, if atmospheric transmission is added to radiance calculations, the amount of error increases and the amount changes for each method. As a general result, among five different methods, the 5th method is chosen the most successful one in many aspects.

If the real image estimation results are considered, it is concluded that at this time, the least amount of error obtained in the 2nd method for Curve Fit and Lookup Table methods, whereas the 5th method gives the best result for the Planck's method. This condition occurs because each estimation method of the camera measures different temperature values for the same frame (in fact, the estimation results of Curve Fit and Lookup Table methods very close to each other). However, if the estimation results including emissivity are evaluated, it can be observed that the temperature value closest to the human skin temperature is again measured by the 5th method.

According to the error analysis of the artificial image, a general condition is observed which is minimum and maximum amount of errors are occurred at the extremum temperature values of the artificial image. However, exceptional cases are also pointed out. The result is also similar for the real image estimations. In order to observe how the amount of error changes between the maximum and minimum temperature limits, the artificial image is used since it is suitable for this investigation because of its particular temperature distribution. Nevertheless, although the error amount can change for different test cases, the behaviour of error distribution and the error amount of the 5th method are the same and very consistent for the all test cases.

According to the estimation results including emissivity, it is observed that the temperature values are increased by 1 °C to 2 °C, if emissivity is included. If the IR camera's results are examined, it is again concluded that different methods measure different temperature values for the same frame.

According to studies, human skin temperature measured at the forehead is determined as around 34 °C [9]. With respect to this reference temperature; results including lower amount of errors than the camera's estimation results obtained in the 5^{th} method with the inclusion of emissivity. The amount of error observed in the 5^{th} method is around 3 °C. This error value contains both the effects of atmospheric transmission and emissivity.

To conclude, in this thesis work, 5 different temperature estimation algorithms are developed and tested on both artificial and real images. Among these methods, the 5^{th} method is come into prominence since it has the lowest amount of errors (≈1 °C) and in addition the error distribution is very consistent for each test case. The results show that including the parameters (i.e. atmospheric transmission, spectral response of the camera detector and emissivity) which affect the radiation coming from any object, better results can be obtained, since the resulting temperature values are found they are quite close to the real temperature values.

REFERENCES

[1] B.R. Lyon, G.L.Orlove, "A Brief History of 25 Years (or more) of Infrared Imaging Radiometers", Proceedings of SPIE Vol. 5073, 2003

[2] A. Rogalski, K. Chrzanowski, "Infrared Devices and Techniques", Optoelectronics Review 10(2), pp. 111-136 (2002)

[3] A.C. Parr, R.U Datla, J.L. Gardner, Optical Radiometry, chapter 1, pg. 1-23, Elsevier Academic Press 2005

[4] W.L. Wolfe, Introduction to Radiometry, chapter 3, pg. 17-19,v. TT29, SPIE Optical Engineering Press, 1998

[5] G. Zissis, The Infrared & Electro-Optical Systems Handbook, Volume 1 – Sources of Radiation, SPIE Optical Engineering Press, 1993

[6] PcModWin Manual, Version 1.4.0, October 2005

[7] User's Manual for ThermaCAM RView, 419-0017-00, August 2007

[8] C. Villasenor-Mora, F.J. Sanchez-Marin, S. Calixto-Carrera, "An Indirect Skin Emissivity Measurement in the Infrared Thermal Range Through Reflection of CO2 Laser Beam", Revista Mexicana De Fisica Vol. 55 (5) 387-392, 2009

[9] F. G. Benedict, W. R. Miles, A. Johnson, "The Temperature Of The Human Skin", April 1919

[10] Thermo Vision SC4000/SC6000 User's Guide, 420-0044-00-10, September 2007

[11] FLIR Systems, http://www.flir.com/thermography/eurasia/en/content/?id=32092, July 2010

APPENDIX

GENERAL SPECIFICATIONS OF THE REFERENCE IR CAMERA

In this thesis work, real image frames have been taken by using a commercial IR camera in order to compare the results of the artificial image and the real image data for the justification of the developed algorithms to work properly. For this purpose, FLIR SC 6000 is chosen and used as a reference IR camera. FLIR SC 6000 and the general specifications of this IR camera are shown in Figure 22 [10] and Table 11 [11], respectively.

Figure 22 –FLIR SC6000 [10]

Table 11 - FLIR SC 6000 General Specifications [11]

Detector & Optics	
Detector Type:	InSb
Spectral Range:	1.5-5μm
Resolution:	640×512
Detector Size:	25μm×25μm
Sensor Cooling:	Stirling closed cycle cooler, optional Liquid Nitrogen
F/#:	2.3
Objective:	50mm, FOV: 18° (h) × 13° (v)
Electronics&Data Rate	
Integration Type:	Snapshot
Integration Time (Electronic Shutter Speed):	9μs to full frame time
Dynamic Range:	14 bit
Data Rate:	50 MHz
Performance	
NEI/NETD:	<25 mK (18mK typical)
Well Capacity:	11 M electrons